



**HAL**  
open science

## The filter-loading effect by ambient aerosols in filter absorption photometers depends on the coating of the sampled particles

Luka Drinovec, Asta Gregoric, Peter Zotter, Robert Wolf, Emily Anne Bruns, André S.H. Prevot, Jean-Eudes Petit, Olivier Favez, Jean Sciare, Ian J. Arnold, et al.

### ► To cite this version:

Luka Drinovec, Asta Gregoric, Peter Zotter, Robert Wolf, Emily Anne Bruns, et al.. The filter-loading effect by ambient aerosols in filter absorption photometers depends on the coating of the sampled particles. *Atmospheric Measurement Techniques*, 2017, 10, pp.1043-1059. 10.5194/amt-10-1043-2017 . ineris-01863156

**HAL Id: ineris-01863156**

**<https://ineris.hal.science/ineris-01863156>**

Submitted on 28 Aug 2018

**HAL** is a multi-disciplinary open access archive for the deposit and dissemination of scientific research documents, whether they are published or not. The documents may come from teaching and research institutions in France or abroad, or from public or private research centers.

L'archive ouverte pluridisciplinaire **HAL**, est destinée au dépôt et à la diffusion de documents scientifiques de niveau recherche, publiés ou non, émanant des établissements d'enseignement et de recherche français ou étrangers, des laboratoires publics ou privés.



## The filter-loading effect by ambient aerosols in filter absorption photometers depends on the coating of the sampled particles

Luka Drinovec<sup>1,2</sup>, Asta Gregorič<sup>3</sup>, Peter Zotter<sup>4,a</sup>, Robert Wolf<sup>4</sup>, Emily Anne Bruns<sup>4</sup>, André S. H. Prévôt<sup>4</sup>, Jean-Eudes Petit<sup>5,6,b</sup>, Olivier Favez<sup>5</sup>, Jean Sciare<sup>6,7</sup>, Ian J. Arnold<sup>8,c</sup>, Rajan K. Chakrabarty<sup>8,d</sup>, Hans Moosmüller<sup>8</sup>, Agnes Filep<sup>9</sup>, and Griša Močnik<sup>1,2</sup>

<sup>1</sup>Research and Development Department, Aerosol d.o.o., Ljubljana, Slovenia

<sup>2</sup>Condensed Matter Physics Department, Jožef Stefan Institute, Ljubljana, Slovenia

<sup>3</sup>Center for Atmospheric Research, University of Nova Gorica, Nova Gorica, Slovenia

<sup>4</sup>Laboratory of Atmospheric Chemistry, Paul Scherrer Institute (PSI), 5232 Villigen PSI, Switzerland

<sup>5</sup>Institut National de l'Environnement Industriel et des Risques (DRC/CARA/CIME), Verneuil-en-Halatte, France

<sup>6</sup>Laboratoire des Sciences du Climat et de l'Environnement (CNRS-CEA-UVSQ), CEA Orme des Merisiers, Gif-sur-Yvette, France

<sup>7</sup>Energy Environment and Water Research Center, The Cyprus Institute, Nicosia, Cyprus

<sup>8</sup>Desert Research Institute, Nevada System of Higher Education, Reno, USA

<sup>9</sup>MTA-SZTE Research Group on Photoacoustic Spectroscopy, Department of Optics and Quantum Electronics, University of Szeged, Szeged, Hungary

<sup>a</sup>now at: Lucerne University of Applied Sciences and Arts, School of Engineering and Architecture, Bioenergy Research, Horw, Switzerland

<sup>b</sup>now at: Air Lorraine, Metz, France

<sup>c</sup>now at: College of Optical Sciences, University of Arizona, Tucson, AZ, USA

<sup>d</sup>now at: Department of Energy, Environmental & Chemical Engineering, Washington University in St. Louis, St. Louis, MO, USA

*Correspondence to:* Luka Drinovec (luka.drinovec@aerosol.si) and Griša Močnik (grisa.mocnik@aerosol.eu)

Received: 2 September 2016 – Discussion started: 13 October 2016

Revised: 27 February 2017 – Accepted: 28 February 2017 – Published: 16 March 2017

**Abstract.** Black carbon is a primary aerosol tracer for high-temperature combustion emissions and can be used to characterize the time evolution of its sources. It is correlated with a decrease in public health and contributes to atmospheric warming. Black carbon measurements are usually conducted with absorption filter photometers, which are prone to several artifacts, including the filter-loading effect – a saturation of the instrumental response due to the accumulation of the sample in the filter matrix. In this paper, we investigate the hypothesis that this filter-loading effect depends on the optical properties of particles present in the filter matrix, especially on the black carbon particle coating. We conducted field campaigns in contrasting environments to determine the influence of source characteristics, particle age and coating on the magnitude of the filter-loading effect. High-

time-resolution measurements of the filter-loading parameter in filter absorption photometers show daily and seasonal variations of the effect. The variation is most pronounced in the near-infrared region, where the black carbon mass concentration is determined. During winter, the filter-loading parameter value increases with the absorption Ångström exponent. It is suggested that this effect is related to the size of the black carbon particle core as the wood burning (with higher values of the absorption Ångström exponent) produces soot particles with larger diameters. A reduction of the filter-loading effect is correlated with the availability of the coating material. As the coating of ambient aerosols is reduced or removed, the filter-loading parameter increases. Coatings composed of ammonium sulfate and secondary organics seem to be responsible for the variation of the load-

ing effect. The potential source contribution function analysis shows that high values of the filter-loading parameter in the infrared are indicative of local pollution, whereas low values of the filter-loading parameter result from ageing and coating during long-range transport. Our results show that the filter-loading parameter can be used as a proxy for determination of the particle coating, thus allowing for differentiation between local/fresh and transported/aged particles.

## 1 Introduction

Black carbon is a primary aerosol tracer for high-temperature combustion emissions and can be used to characterize the time evolution of its sources (Lack et al., 2014). Investigations performed on ambient black carbon (BC) mass equivalent concentrations have shown a stronger correlation with adverse public health effects than the ones observed for the total mass of particulate matter (Janssen et al., 2011, 2012; Grahame et al., 2014; Olstrup et al., 2016). Black carbon absorbs sunlight very efficiently and heats the atmosphere with the top-of-the-atmosphere forcing exceeding  $1 \text{ W m}^{-2}$ , and even though its lifetime is short compared to  $\text{CO}_2$ , it is still the second-most-important warming agent (Bond et al., 2013). Models show that its short lifetime opens up the possibilities for short-term mitigation of atmospheric warming (Shindell et al., 2012). While health effects are of interest in the context of local air pollution, climate change is investigated on regional and global scales, and co-benefits from black carbon emission reductions are of great interest (Smith et al., 2009). Measurements are conducted at locations suitable for all three different scales, with absorption filter photometers being the most common instrumentation employed to determine ambient black carbon mass concentrations.

Filter photometers measure the change of light transmitted by or reflected from the fiber filter on which particles are collected. These methods feature high sensitivity and high time resolution. The measurements, however, depend on the multiple light scattering within the filter and are prone to several artifacts, including filter-loading effect and particle scattering (Lack et al., 2014). Herein we focus on the filter-loading effect (FLE), a saturation of the instrumental response due to the accumulation of the sample in the filter matrix (Bond et al., 1999; Weingartner et al., 2003; Moosmüller et al., 2009). This nonlinearity depends on the filter material and the type of instrument (Virkkula et al., 2007; Collaud Coen et al., 2010; Hyvärinen et al., 2013). It is important to compensate for FLE to obtain accurate measurements of black carbon concentration and for the determination of aerosol absorption spectra, which are used for source apportionment (Kirchstetter et al., 2004; Sandradewi et al., 2008).

The filter-loading effect – that is, the reduction of the measurement sensitivity with increasing filter loading – in Aethalometers has been described by several models (Wein-

gartner et al., 2003; Arnott et al., 2005; Schmid et al., 2006; Virkkula et al., 2007; Park et al., 2010; Collaud Coen et al., 2010; Drinovec et al., 2015). Offline methods for the quantification of FLE are based on jumps of reported BC values just before and immediately after the filter change (Weingartner et al., 2003; Virkkula et al., 2007) or the BC vs. ATN method (Park et al., 2010; Segura et al., 2014; Drinovec et al., 2015). These low-time-resolution estimations of FLE showed big differences in the effect between seasons (Virkkula et al., 2007). Uncoated soot induces a higher loading effect compared to coated soot (Weingartner et al., 2003), and Virkkula et al. (2015) showed that the loading parameter depends on the backscatter fraction and the single-scattering albedo (SSA).

Traditionally, Aethalometer data have been post-processed using fixed parameters characterizing the loading effect. With the introduction of the dual-spot Aethalometer it has become possible to measure FLE with high time resolution (Drinovec et al., 2015). This allows for a much better characterization of effects governing FLE. In this paper, we are testing the hypothesis that the filter-loading effect depends on the optical properties of particles present in the filter matrix, especially on black carbon particle coating. Under laboratory conditions, coating can enhance optical absorption of soot particles by up to factor of 2 (Weingartner et al., 2003; Schnaiter et al., 2003). Ambient experiments show a smaller effect from 6 to 60 % (Cappa and Wilson, 2012; Moffet and Prather, 2009; Liu et al., 2015). Determination of the mixing state using FLE may also reduce uncertainties in radiative forcing estimates (Jacobson, 2001; Shiraiwa et al., 2008). There are two extreme mixing state models: an internal and an external mixture as defined by Seinfeld and Pandis (2006), where the external mixture represents two separate populations of two types of particles and where an internal mixture represent one population of particles composed of a homogeneous mixture of materials from the two types. Because black carbon cannot be homogeneously mixed with non-absorbing material, a third mixing state was introduced: a core-shell state (Jacobson, 2000). We use the term “mixing state” to refer to either of these states, most notably the external and the core shell.

We conducted field campaigns in contrasting environments to determine the influence of sources, particle age and coating on the magnitude of the FLE. We show that the FLE during the 1-year-long campaign in Paris features distinct winter and summer patterns. Winter dependence of the FLE is discussed in the context of presented laboratory experiments with BC of different particle size. Winter and summer intensive campaigns in Paris and Payerne allowed us to determine a coating factor, which represents the relative contribution of the material available for coating. The FLE behavior during summer reveals an influence of particle coating on the FLE. As particles get coated by secondary material during atmospheric ageing, we show, using back-trajectory analysis, that the FLE depends on the particle age. The ambient

campaign in Ljubljana quantifies the increase of the loading effect when the particle coating is removed.

## 2 Materials and methods

### 2.1 Instrumentation

BC and absorption coefficients are characterized with the dual-spot Aethalometer (Magee Scientific Aethalometer model AE33) with real-time loading compensation (Drinovec et al., 2015). The inlet air stream of the AE33 is split, and the sample is collected on two filter spots concurrently within the instrument. The flow through each of the two spots is different, so the loading rates on the respective sample spots are different. Different loading rates cause the accumulation of the sample to be different between the two spots, resulting in a different magnitude of FLE between the spots. Measurement of FLE enables the compensation of the data – using the parametrization described in Drinovec et al. (2015), the compensation parameter  $k$  can be derived. This parameter describes the linear decrease of the instrumental sensitivity with loading of the spot with the absorbing sample for each wavelength of light at which the measurement is performed. The absorption coefficients are calculated at all wavelengths, and BC is determined from the measurement at the wavelength 880 nm. Absorption and BC are compensated using the following equation:

$$BC_{\text{compensated}}^{\lambda} = \frac{BC_{\text{non-compensated}}^{\lambda}}{(1 - k_{\lambda} \times ATN_{\lambda})}, \quad (1)$$

where ATN is optical attenuation of light passing through a sample loaded filter.  $k_1, k_2, k_3, k_4, k_5, k_6$  and  $k_7$  are compensation parameters determined at the following wavelengths: 370, 470, 520, 590, 660, 880 and 950 nm, respectively. The absorption Ångström exponent (AAE) (Ångström, 1929) is calculated from absorption coefficient  $b$  (Drinovec et al., 2015) measured at 470 and 950 nm:  $AAE = \ln(b_{470 \text{ nm}}/b_{950 \text{ nm}})/\ln(950/470)$ . The instruments were run at  $5 \text{ L min}^{-1}$  total sample flow and 1 min time resolution.

The measurement of non-refractory submicron (NR-PM<sub>1</sub>) major chemical species (i.e., organic matter, nitrate, sulfate, ammonium and chloride) was performed using an Aerodyne<sup>®</sup> aerosol mass spectrometer (AMS) and/or an aerosol chemical speciation monitor (ACSM), fully described elsewhere (Canagaratna et al., 2007; Ng et al., 2011; Fröhlich et al., 2013). Briefly, PM<sub>2.5</sub> aerosols are sampled at  $3 \text{ L min}^{-1}$  and then sub-sampled at about  $85 \text{ mL min}^{-1}$  through an aerodynamic lens, focusing submicron particles onto a  $600^{\circ}\text{C}$  heated conical tungsten vaporizer where non-refractory material is flash-vaporized and quasi-instantaneously ionized by electron impact at 70 eV. The AMS mainly differs from the ACSM system by allowing for size-segregated measurements of the chemical composition by using a chopper in the AMS. Many AMSs also use ad-

vanced mass spectrometers with higher resolution and better detection limits. However, for the measurements of NR-PM<sub>1</sub> species in ambient air, a good agreement is commonly observed between data from these two instruments (Crenn et al., 2015; Fröhlich et al., 2015).

Individual aerosol particles were analyzed using a field emission gun scanning electron microscope (FEG SEM, JEOL JSM 7100F TTLS) coupled with an energy-dispersive X-ray (EDX) system (X-Max Large Area Analytical Silicon Drift Detector, Oxford Instrument). Aluminum foils used for sampling of aerosol particles (sampling described in Sect. 2.2) were mounted directly on the sample holder by double-sided conductive carbon tape. SEM-EDX acquisitions were performed under high vacuum at 5 keV accelerating voltage. Micrographs were acquired by a secondary electron detector at 4–6 mm working distance (WD). The samples were first scanned under low magnification to obtain the overall distribution of the particles and afterwards closely examined at magnifications from 10 000 to 50 000 $\times$ . Representative areas were chosen for further EDX analysis, which was focused on the identification of the coating material of soot agglomerates. The microanalysis was performed at 10 mm WD with acquisition time of 50 to 150 s. Since the spatial resolution of the EDX analyses is around 1  $\mu\text{m}$ , the obtained results were considered as a qualitative assessment of particle elemental composition.

### 2.2 Measurement campaigns

The Paris campaigns were conducted at the SIRTA observatory located about 20 km south of Paris, France ( $48^{\circ}42'47'' \text{ N}$ ,  $2^{\circ}12'29'' \text{ E}$ ). The observatory sits on a plateau, about 160 m a.s.l., in a semi-urban environment being divided between agricultural fields, wooded areas, housing and industrial developments. The prevailing winds are from the southwest, blowing air of maritime origin over the site (e.g., Crippa et al., 2013). Northeasterly winds also occur quite frequently under high-pressure systems. The latter conditions are associated with the advection of continental air masses as well as of polluted air from the Paris metropolitan area. Beside continuous AE33 and ACSM measurements since 2013, results from two intensive European Monitoring and Evaluation Programme (EMEP) campaigns in summer 2012 (15 June–10 July 2012) and winter 2013 (24 January–16 February 2013) were available for the present study.

The Payerne station is a rural background air quality monitoring station located in southwestern Switzerland ( $46^{\circ}48'47'' \text{ N}$ ,  $6^{\circ}56'40'' \text{ E}$ , 489 m a.s.l.), between the Jura and the Alps. It is situated about 1 km southeast of the small rural town of Payerne (Switzerland). The site is surrounded by agricultural land (grassland and crops), forests and small villages. Intensive campaigns took place in summer (15 June 2012–10 July 2012) and winter (24 January 2013–16 February 2013). In addition to the Aethalometer

AE33, a high-resolution ToF-AMS (Aerodyne Research) was operated throughout the campaigns.

The Ljubljana campaign was held between 6 August 2014 and 12 September 2014 in a suburban background location, 10 km southwest of Ljubljana, Slovenia (46°0′58″ N, 14°24′42″ E, 293 m a.s.l.). The site is at the edge of a village surrounded by agricultural fields and at a distance of 500 m from a highway. It lies in the Ljubljana basin, which is surrounded by hills rising from 500 to 1700 m above the valley floor. The Ljubljana campaign used four AE33 Aethalometers measuring four different ambient air streams: non-treated, dried, thermodenuded, and thermodenuded and dried samples. Ambient, dried and thermodenuded air streams had separate inlets; the thermodenuded sample was separated in two streams, one connected directly to the Aethalometer and the second guided through a silica gel drier. The Dekati thermodenuder was set to a temperature of 300 °C with 10 L min<sup>-1</sup> sample flow, which was split for the two Aethalometers. The thermodenuder consists of a heated section and an air-cooled denuder where semi-volatile compounds are adsorbed onto activated charcoal. The estimated residence time for 10 L min<sup>-1</sup> flow was 0.5 s. A diffusion membrane drier (Magee Scientific, Aerosol Inlet Dryer) and a silica gel drier with dew point reductions of 11.0 ± 1.0 and 11.5 ± 1.0 °C, respectively, were used. A scanning mobility particle sizer (SMPS) with a differential mobility analyzer (DMA) (TSI, Model 3080) connected to a water-based condensation particle counter (CPC) (TSI, Model 3785 UWCPC) was used to acquire the particle size distribution every 5 min. A Dekati low-pressure impactor (DPLI) was used to sample particles into 13 size fractions (from 30 nm to 10 µm) for SEM and EDX spectroscopy analysis. Impactor samples were collected on aluminum foils (Dekati, CF-300) covered by a thin layer of Apiezon L grease. Impactor stage 4 with an expected particle size range between 170 and 260 nm was analyzed.

The K-puszta campaign took place at the K-puszta observatory (Hungary, 46°58′12″ N, 19°33′ E, 125 m a.s.l.) during January and February 2013. During winter ambient aerosols are dominated by wood burning emissions from household heating. The laboratory biomass burning profile was obtained during an experiment performed at the Paul Scherrer Institute (Bruns et al., 2015). Laboratory diesel exhaust was characterized at Aerosol d.o.o. in Ljubljana from a Euro 3 diesel engine. The exhaust was transferred into the smog chamber, where it was diluted and analyzed. Ljubljana roadside measurements were conducted during November 2012 in the city center, close to a heavy-traffic road.

The Reno laboratory experiment was conducted at Desert Research Institute (Reno, Nevada, USA). Pure mustard oil was burned in a simple ceramic bowl with a cotton wick. The diluted emissions were collected and injected into a distribution chamber (50 L) from which the sample was routed to multiple instruments: the Aethalometer model AE33 run at 1 s time resolution, the Photoacoustic Soot Spectrometer

(model PASS-3, Droplet Measurements Technologies) operated at 2 s time resolution, and the SMPS (TSI, DMA model 2080 with CPC model 3775). Ponderosa pine needles (~ 50 g) were combusted in a biomass combustion chamber, a close replica of which has been described by Tian et al. (2015). The combustion process could be divided into the flaming and smoldering phases. Focusing on the flaming phase, we injected the emissions from the first 35 s of the combustion into the distribution chamber. The sample from the distribution chamber was analyzed for approximately 15 min (time series of BC is shown in Supplement Sect. S.6). PASS-3 absorption and scattering measurements were used to calculate the SSA (Lewis et al., 2008).

### 2.3 Trajectory analysis

To illustrate air mass origin during specific pollution episodes during the Paris and Payerne campaigns (please see Sect. 2.2), 72 h back trajectories were calculated every 3 h using the PC-based version (v.4.9) of HYSPLIT (Stein et al., 2015) with weekly Global Data Assimilation System (GDAS) meteorological field data. Back trajectories were set to end at SIRTa and Payerne at 500 m above ground level (a.g.l.).

The potential contribution source function (PSCF) was used to investigate the potential advection of particulate material over large geographical scales during the different measurement campaigns. In this methodology, the probability that an air parcel may be responsible for high concentrations measured at the receptor site is calculated based on back-trajectory analyses, as described in Polissar et al. (1999). Briefly, at each *ij*th grid cell, probabilities are calculated as

$$\text{PSCF}_{ij} = \frac{m_{ij}}{n_{ij}}, \quad (2)$$

where *n<sub>ij</sub>* represents the total number of back trajectories passing through each *ij*th cell, and *m<sub>ij</sub>* the number of back trajectories passing through the same cell that are associated with measured concentrations higher than a user-defined threshold. A 0.5° × 0.5° grid cell was used, covering western Europe. Similarly to Waked et al. (2014), wet deposition was roughly estimated with precipitation data along each trajectory, assuming that even low precipitation would clean up the air parcel. For graphical purpose, results were smoothed by a Gaussian filter and eventually normalized (see Fig. 9 with color scales from 0 to 1).

## 3 Results

### 3.1 Variability of filter-loading effect

The magnitude of the FLE for aerosols collected on a filter is dynamically determined by the dual-spot Aethalometer (Drinovec et al., 2015). The FLE depends on the entirety of the sample accumulated in the filter matrix up to the time of the

**Table 1.** Typical wavelength dependence of the filter-loading compensation parameter  $k$  obtained for ambient and laboratory campaigns. Campaign average  $k$  and absorption Ångström exponent (AAE) are presented. The 590 nm channel data for Payerne summer were not available (NA) due to instrument malfunction.

		K-pusztza winter	Laboratory biomass burning	Payerne winter	Laboratory diesel engine exhaust	Ljubljana roadside	Paris summer	Payerne summer
AAE		1.55	1.40	1.35	1.04	0.97	1.06	1.16
Filter-loading parameter $k$ at the wavelength	370 nm	0.0047	0.0046	0.0044	0.0041	0.0045	0.0041	0.0043
	470 nm	0.0055	0.0052	0.0049	0.0045	0.0048	0.0036	0.0039
	520 nm	0.0059	0.0056	0.0051	0.0046	0.0050	0.0035	0.0038
	590 nm	0.0067	0.0060	0.0055	0.0048	0.0051	0.0034	NA
	660 nm	0.0072	0.0063	0.0059	0.0050	0.0052	0.0032	0.0034
	880 nm	0.0081	0.0072	0.0063	0.0055	0.0052	0.0024	0.0019
	950 nm	0.0084	0.0074	0.0064	0.0056	0.0053	0.0023	0.0012

measurement. The value of the FLE compensation parameter  $k$  is calculated for each of the seven measurement wavelengths, yielding a specific spectral fingerprint, which differs substantially between different measurement campaigns (Fig. 1). The campaign-averaged values of the loading parameter  $k$  for short wavelengths show limited variability with a range of 0.004–0.005, while the variability in the near infrared is much greater with a range of 0.001–0.008 (Table 1 and Fig. 1).

Table 1 also reports the average values of the absorption Ångström exponent obtained for each campaign. Occurrence of higher  $k$  values appears to be linked to higher values of the absorption Ångström exponent, which is commonly used as a tracer for biomass burning aerosols (Kirchstetter et al., 2004; Sandradewi et al., 2008). This is evident for both laboratory and ambient data, with the most extreme case for field campaigns being K-pusztza winter data. For fresh diesel exhaust (laboratory and Ljubljana roadside measurements), the obtained  $k$  values fall in the middle of the parameter range, whereas lower  $k$  values are obtained for the summer ambient (Paris and Payerne) campaigns. This variability will be investigated in more detail in the following section.

### 3.2 Seasonal variation of filter-loading effect

One-year-long black carbon mass concentrations at SIRTAs show significant day-to-day variability with yearly average and standard deviation of  $1068 \pm 1123 \text{ ng m}^{-3}$  (Fig. 2). Average concentrations are  $913 \pm 932$  and  $1263 \pm 1299 \text{ ng m}^{-3}$  for the hot (April–September) and cold (October–March) periods, respectively. The sources of black carbon impacting the measurement site vary during the year; during summer the AAE is close to 1, indicating the dominance of traffic emissions, while during winter its value is 1.4, suggesting the importance of biomass burning from residential heating (Kirchstetter et al., 2004; Sandradewi et al., 2008), which is consistent with previous BC source apportionment studies performed in the Paris area during intensive campaigns

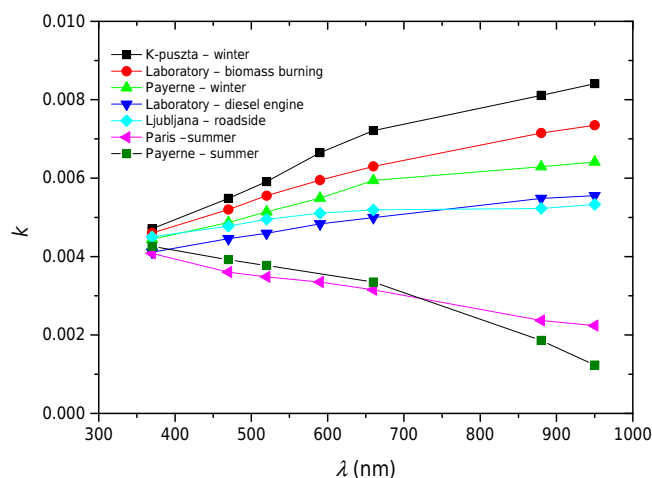


**Figure 1.** Typical spectral fingerprints of the FLE compensation parameter  $k$  obtained during ambient and laboratory campaigns. Campaign/experiment average values are presented.

(e.g., Favez et al., 2009; Petit et al., 2014) as well as long-term investigations (Petit et al., 2015).

Concomitantly with the absorption Ångström exponent, the parameter  $k$  shows large seasonal variations (Figs. 3 and 4). Virkkula et al. (2015) analyzed the  $k$  wavelength dependence by calculating the slope of  $k$  vs.  $\lambda$ . It was shown that the slope is extremely well correlated with the compensation parameter  $k_6$  (measured at 880 nm), so either of the two can be used to describe the variation of the parameter  $k$ . For the sake of simplicity, we focus our further analysis on  $k_6$ . High values of  $k_6$ , between 0.006 and 0.012, are observed during winter, while in summer  $k_6$  remains low, featuring still large oscillations (0–0.005), with episodes of low  $k_6$  that can last for several days, indicating stronger influence of weather conditions than of daily cycles.

Figure 4 shows monthly spectral fingerprints of the parameter  $k$ , which are in agreement with the offline analy-

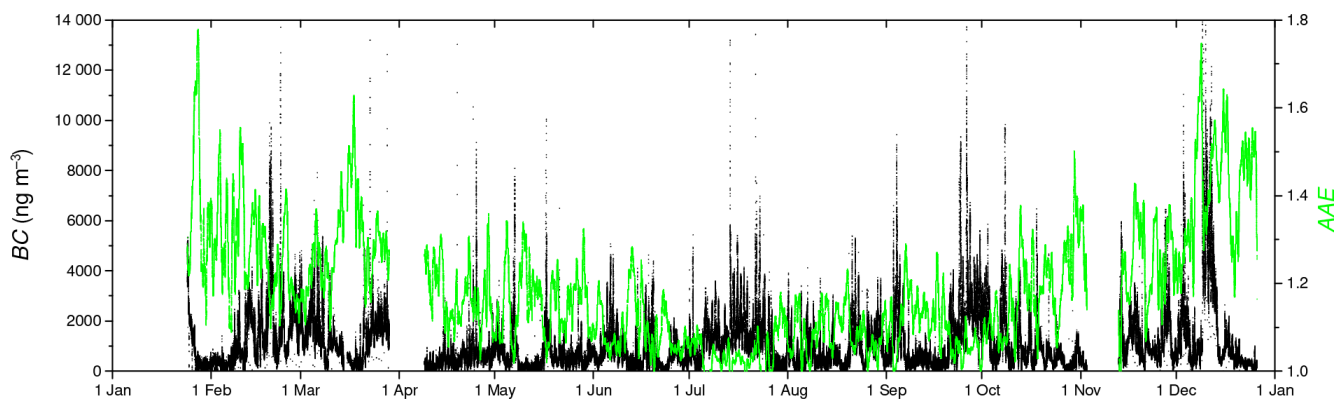


**Figure 2.** Black carbon mass concentration and AAE measured at the Paris urban background site (SIRTA observatory) during 2013.

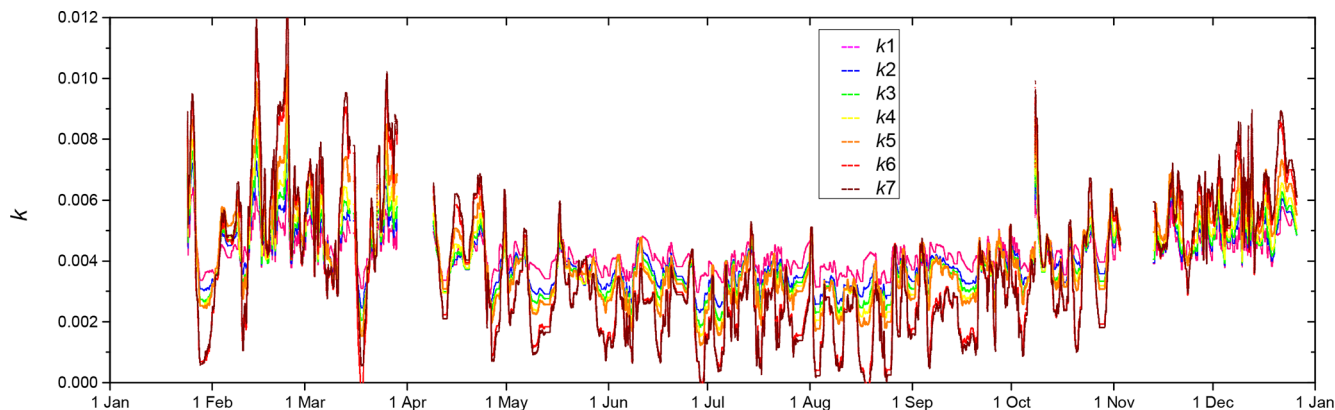


**Figure 3.** Filter-loading parameter  $k$  measured at the Paris urban background site (SIRTA observatory) in 2013.

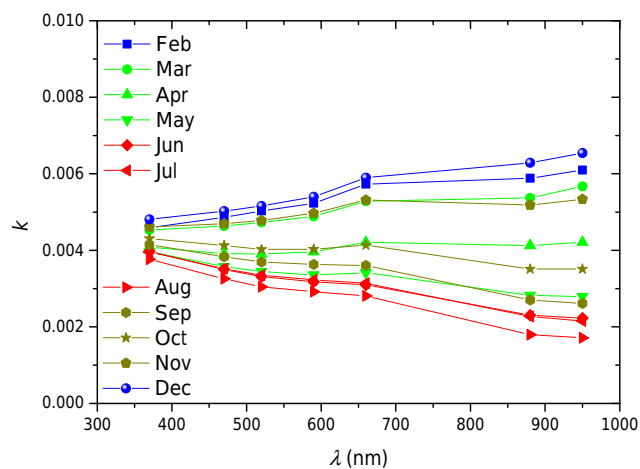


**Figure 4.** Monthly spectral fingerprints of the filter-loading effect compensation parameter  $k$ , obtained during the Paris campaign (SIRTA observatory) in 2013.

sis of the Aethalometer data (Virkkula et al., 2007, 2015): we measured the lowest values of the parameter  $k$  during summer (red) and highest during winter (blue) months, with

spring and autumn somewhere in between. Again, the variation of the parameter  $k_6$  roughly correlates with the AAE, except for the months of April, May and October, when the  $k_6$  monthly mean varies between 0.0028 and 0.0041, while the AAE mean changes very little between these months (Table 2 and Fig. S5 in the Supplement). This seems to indicate that two distinct factors – meteorology and sources – may significantly influence the value of the parameter  $k$ .

To analyze the influence of black carbon sources, we investigated in more detail the dependence of  $k_6$  on the AAE during the heating season. The November–December period was analyzed because of stable weather conditions. The results confirm that for AAE values above 1.2 the loading parameter  $k_6$  increases with AAE (Fig. 5), indicating higher values for biomass burning emissions than traffic emissions. This is in agreement with the laboratory biomass burning experiment, where high  $k_6$  values were also obtained (Fig. 1). Figure 5 shows a value for  $k_6$  close to 0.0055 at an absorption Ångström exponent of 1, as expected for diesel exhaust from source and ambient measurements (Table 1). We hypothesize that higher values of  $k_6$  for biomass burning compared to diesel exhaust are related to the difference in black carbon agglomerate size, which is investigated in more detail

**Table 2.** Monthly averages and standard deviation of black carbon (BC) mass concentration, AAE and compensation parameter  $k_6$  for the Paris campaign (SIRTA observatory) in 2013.

Month	BC ( $\text{ng m}^{-3}$ )	AAE	$k_6$
February	$1390 \pm 1320$	$1.28 \pm 0.47$	$0.0059 \pm 0.0023$
March	$1370 \pm 1070$	$1.29 \pm 0.23$	$0.0054 \pm 0.0024$
April	$570 \pm 640$	$1.17 \pm 0.43$	$0.0041 \pm 0.0016$
May	$640 \pm 660$	$1.16 \pm 0.46$	$0.0028 \pm 0.0011$
June	$750 \pm 670$	$1.10 \pm 0.37$	$0.0023 \pm 0.0010$
July	$1250 \pm 1000$	$1.04 \pm 0.31$	$0.0023 \pm 0.0010$
August	$870 \pm 690$	$1.09 \pm 0.32$	$0.0018 \pm 0.0012$
September	$1310 \pm 1380$	$1.10 \pm 0.29$	$0.0027 \pm 0.0010$
October	$960 \pm 910$	$1.18 \pm 0.33$	$0.0035 \pm 0.0015$
November	$1180 \pm 950$	$1.25 \pm 0.25$	$0.0052 \pm 0.0009$
December	$1580 \pm 1930$	$1.41 \pm 0.26$	$0.0063 \pm 0.0010$

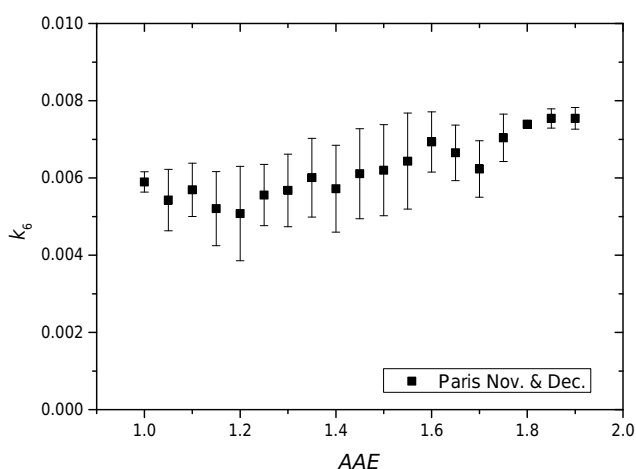


**Figure 5.** Correlation between the FLE compensation parameter  $k_6$  and the AAE for November and December 2013 in Paris (SIRTA observatory).

in the following section. Indeed, the diesel engine exhaust soot mobility diameter was reported in the 30–100 nm range (Harris and Maricq, 2001; Keskinen and Rönkkö, 2010; Ning et al., 2013), in contrast to the 130–160 nm range for woodstove emissions (Laborde et al., 2013) and 260–590 nm for wildfires (China et al., 2013). In special cases of large-scale sooty and turbulent fires with long flame residence time it is possible to obtain super-aggregates with geometric diameter larger than 1  $\mu\text{m}$  (Chakrabarty et al., 2014).

### 3.3 Particle size and the filter-loading effect

To investigate the influence of black carbon particle size on  $k$ , we characterized emissions from a mustard oil lamp and from flaming ponderosa pine (*Pinus ponderosa*) needle combustion under laboratory conditions. Mustard oil burning produces particles with a mode of mobility number size distribution of 210 nm (Fig. 6b), which compares fairly well

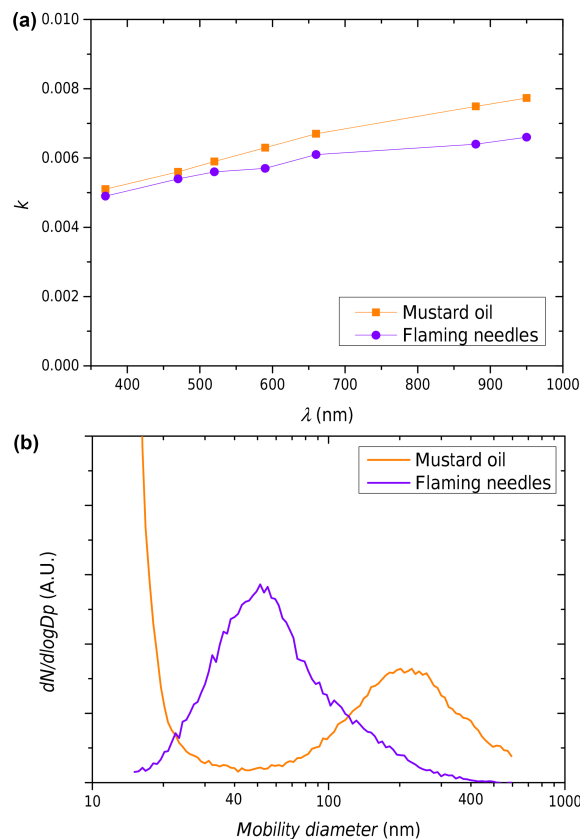


**Figure 6.** Filter-loading parameter  $k$  for laboratory measurements of emissions from mustard oil lamp and flaming Ponderosa pine needles (a). Normalized aerosol number size distributions for both sources (b).

with the median aggregate mobility diameter of  $297 \pm 74$  nm reported by Chakrabarty et al. (2013) for mustard oil lamp emissions. These particles are dominated by black carbon as indicated by an absorption Ångström exponent of 1 and low single-scattering albedo of 0.222 (Table 3). Our Ångström exponent of 1 (470, 950 nm) is somewhat lower than that determined by Chakrabarty et al. (2013, Fig. 2a) as  $1.331 \pm 0.004$  (405, 781 nm) with a three-wavelength photoacoustic instrument. Our single-scattering albedo is in agreement with the lower values of 532 nm SSA measured by Chakrabarty et al. (2013, Fig. 4a) with an integrated photoacoustic nephelometer. Chakrabarty et al. (2013) argue that higher values (up to  $\sim 0.8$ ) of single-scattering albedo shown in their Fig. 4 were caused by flickering of the flame increasing organic matter emissions, which may also have caused their increased absorption Ångström exponents. Flaming pine needle combustion produces considerably smaller particles with a mean diameter of 50 nm. We sampled only the flaming phase of Ponderosa pine needle combustion, where the emissions feature low values of the AAE (i.e., 1.25) and SSA (i.e., 0.43) as shown in Table 3. This is in agreement with the low SSA of  $0.41 \pm 0.14$  at 532 nm that can be de-

**Table 3.** Filter-loading parameter  $k_6$ , aerosol mobility diameter (mode of number size distribution), single-scattering albedo (SSA) at 532 nm and AAE of soot generated by mustard oil lamp and flaming Ponderosa pine needles.

	$k_6$	Particle size mode (nm)	SSA <sub>532 nm</sub>	AAE
Mustard oil lamp	$0.0074 \pm 0.0003$	210	$0.222 \pm 0.003$	$1.02 \pm 0.02$
Flaming needles	$0.0064 \pm 0.0014$	50	$0.43 \pm 0.05$	$1.25 \pm 0.03$

rived from the ratio of fuel-based emission factors of absorption and extinction cross sections measured by Chen et al. (2007, Table 1) with a photoacoustic absorption instrument and a cavity ring-down (CRD)/cavity-enhanced detection (CED) extinction instrument, respectively, for flaming combustion of Ponderosa pine needles. We observed a larger filter-loading effect for mustard oil lamp emissions (Fig. 6a), which we believe is related to the larger particle size. This might explain the correlation between  $k$  and AAE in Fig. 5. The values of the loading parameter for both sources and their wavelength dependence are similar to the ambient observations in winter (Figs. 1 and 4). The loading parameter values for fresh combustion products seem to be influenced by the size of the combustion products, with an approximately 15 % increase in the infrared (IR) wavelength region for an aerosol mobility diameter increase of about 4 times. The increase of the loading parameter in the IR with size is consistent with the reported soot particle diameters for different ambient sources (Ning et al., 2013; China et al., 2013). The difference in size is accompanied by the difference in the absorption Ångström exponent and single-scattering albedo. In addition to the size dependence of  $k_6$ , the dependence of the loading parameter on SSA we report here agrees with the one reported for Nanjing (Virkkula et al., 2015) – the decrease in SSA increases the loading parameter.

### 3.4 Influence of the mixing state on the filter-loading effect: material available for coating

The second factor influencing  $k$  was assumed to be related to the meteorological conditions. To test this assumption, high-time-resolution variation of  $k$  was investigated during EMEP campaigns taking place during summer and winter in Paris and Payerne (Fig. S1). During summer, we observed periods with  $k_6$  close to 0, which lasted for several days with short intervals with  $k_6$  close to 0.005. During the winter campaigns, we observed higher values of  $k_6$  (up to 0.01) at both locations, whereas in Paris there were also two periods with low  $k_6$  values. To investigate the dependence of the loading parameter  $k$  on the available coating material, we combined the Aethalometer data with the Payerne and Paris AMS/ACSM data. Here we define the coating factor (CF) as a mass of the potential material available for coating (a sum of sulfate, ammonium, nitrate and organic mass) normalized to the black carbon mass:

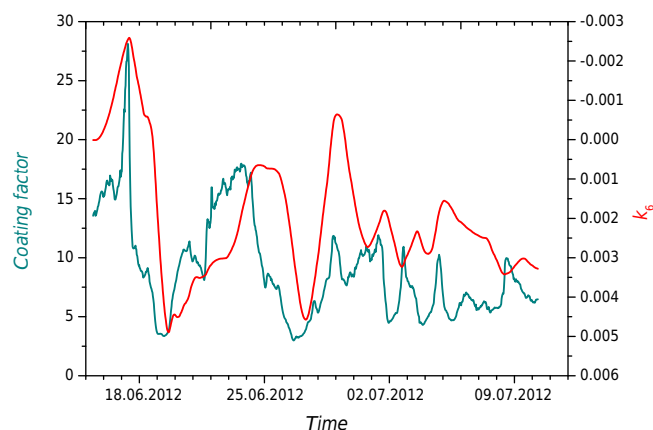


**Figure 7.** Coating factor (CF) and filter-loading parameter  $k_6$  time series during the Paris summer campaign. Note the inverted scale for  $k_6$ .

$$\text{CF} = \frac{(\text{SO}_4^{2-} + \text{NO}_3^- + \text{NH}_4^+ + \text{ORG})}{\text{BC}} \quad (3)$$

The time series of CF and  $k_6$  from the Paris summer campaign shows a similar time variation pattern (Fig. 7). High CF coincides with low value of parameter  $k_6$ , and vice versa. However, there is a time lag between both measurements which is related to the way the loading parameter  $k$  is determined (Drinovec et al., 2015): the parameter  $k$  is a cumulative property of all particles on the filter; hence all particles on the filter, collected from the last time the tape has been advanced, contribute to the loading effect. This means that the time lag varies with and depends on the ambient black carbon concentration. The second reason is the geometric smoothing employed in the algorithm, which takes the last  $k$  value determined from the previous filter spot into account. The time lag impairs the  $k_6$  vs. CF correlation resulting in a higher standard deviation of  $k_6$  averaged in each CF bin (Fig. 8).

We have observed a change of  $k_6$  with increasing coating factor for all four campaigns. The decrease is of different magnitude and shape for summer and winter. The decrease is larger in summer than in winter. In summer in Paris and in Payerne in both seasons, the relationship is linear, while the shape is more complex in Paris in winter.

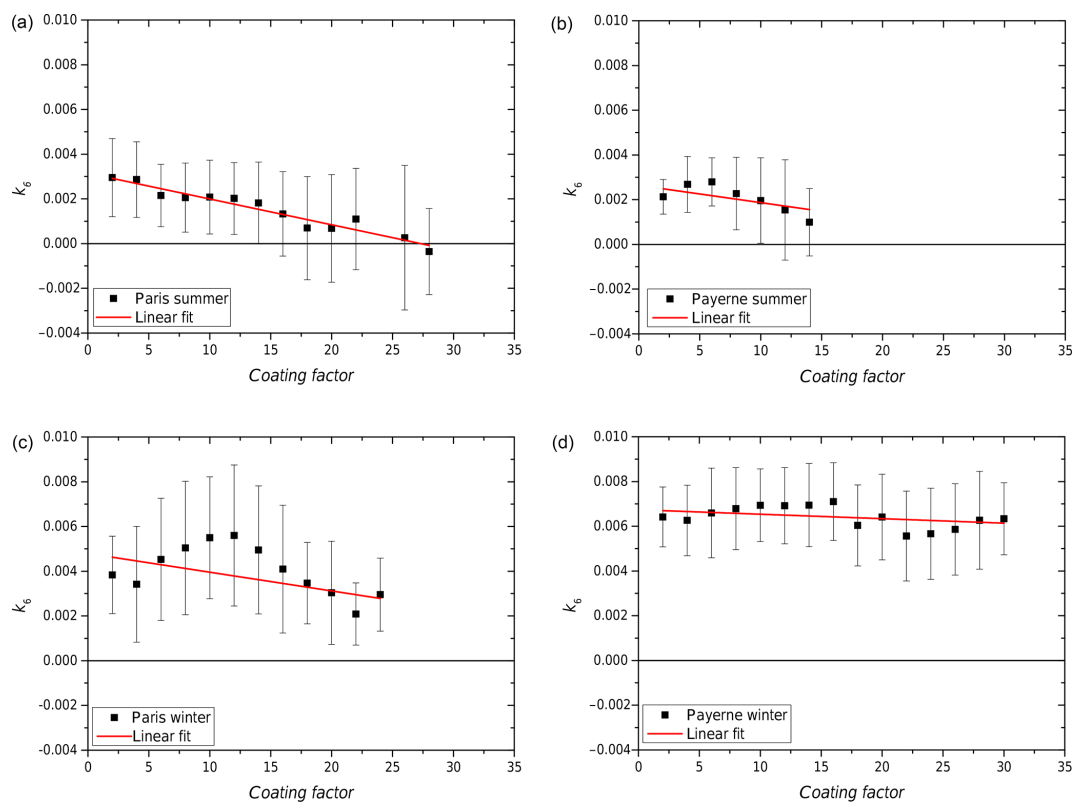


**Figure 8.** Correlation between the filter-loading parameter  $k_6$  and the CF during winter and summer campaigns in Paris and Payerne. Hourly data are averaged in CF bins 2 units wide. The error bars represent standard deviation for data points inside each bin.

**Table 4.** Fitting parameters of the filter-loading parameter  $k_6$  versus the coating factor and AAE during winter and summer campaigns in Paris and Payerne.

	slope ( $10^{-4}$ )	intercept at $k_6 = 0$	AAE
Paris summer	$-1.2 \pm 0.1$	$27 \pm 3$	1.06
Payerne summer	$-0.8 \pm 0.5$	$35 \pm 20$	1.16
Paris winter	$-0.8 \pm 0.3$	$57 \pm 22$	1.34
Payerne winter	$-0.2 \pm 0.1$	$340 \pm 180$	1.35

The results are most pronounced for the Paris summer campaign with the largest absolute slope of the linear regression line. In Payerne in summer, the slope is slightly lower. In summer,  $k_6$  reaches 0 at coating factor values of approximately 30 for both locations (Table 4). These results show that during summer the coating material causes a reduction of the filter-loading effect. In Paris, CF is much larger than it is in Payerne. Because most of the non-refractory material in Paris during the summer is of secondary origin (Freutel et al., 2013), it is possible to form internally mixed aerosols in the atmosphere. The correlation of particle size with coating factor in Paris supports this assertion (Fig. S2).

The fitted slope obtained for the Paris winter campaign is lower compared to summer, and  $k_6$  reaches 0 at  $CF = 57$ , with the dependence being more complicated than the linear one observed in summer. There is almost no decrease of  $k_6$  with increasing CF during winter in Payerne. This might be a consequence of biomass burning emissions which are dominated by organics usually externally mixed with black carbon – as confirmed for the Paris region during the MEGAPOLI campaign (Healy et al., 2013). The amount of black carbon and organics from biomass burning depends strongly on the combustion conditions, with black carbon being created at high-temperature flaming combustion and organics at low-temperature smoldering combustion (Chakrabarty et al., 2013; Pagels et al., 2013). Especially during summer, elevated amounts of secondary non-refractory material are available for coating, and we observe a good correlation of  $k_6$  with CF, which indicates that coating is responsible for reduction of the filter-loading effect. The decrease of  $k_6$  with increasing CF is at first counterintuitive when it is compared with the influence of the measured aerosol mobility diameter on  $k_6$ . It was observed that the increase in the mobility diameter may induce a  $k_6$  increase (Fig. 6), and one could speculate that the availability of material for coating black carbon cores, and hence a high value of CF, would increase the aerosol size and thereby increase the  $k_6$  value. In fact,

the contrary happens; increasing CF decreases  $k_6$ . However, increase in CF should increase SSA as well, and it has been shown for ambient aerosols in Nanjing (Virkkula et al., 2015) that the increase in SSA decreases  $k_6$ . To resolve this question in the following sections, we will investigate first the influence of aerosol age and continue with removing or reducing aerosol coating.

### 3.5 Aerosol age and origin influence the filter-loading effect

The influence of the aerosol age was indirectly investigated by using the PSCF. We divided the dataset into two subsets distinguished by  $k_6$  being bigger or smaller than the campaign average of 0.002. The analysis was carried out for the summer period at Paris and Payerne (Fig. 9). For both sites,  $k_6 > 0.002$  and  $k_6 < 0.002$  occurred around 60 and 40 % of the time, respectively. There are sufficient data in both subsets to provide comparable results. In Paris, the compensation parameter  $k$  is very well correlated with aerosol age: high values indicate local sources, while values close to 0 indicate long-range transport (Fig. 9). High  $k_6$  values are associated with a local pattern of air pollution, since the highest PSCF values are located near the station. The map resembles results previously obtained in Paris for local sources like traffic and wood burning (Bressi et al., 2014). Measurements during the MEGAPOLI campaign showed that fresh traffic BC particles are non-coated, whereas BC particles from long-range transport exhibit substantial coatings of non-refractory material (Laborde et al., 2013). For low  $k_6$  values ( $k_6 < 0.002$ ) the sources are distributed over France, part of Great Britain and the Atlantic Ocean. PSCF results for CF follow the same pattern, indicating a potential coating material that is brought to Paris by mid- and long-range transport during which the emissions are aged and aerosols get coated, and also mixed with more local sources of BC (Bressi et al., 2013; Petit et al., 2015).

Theoretical studies show that coating consisting of secondary organic and inorganic species is mostly transparent in the visible part of the spectrum and can affect the absorption of light by the particles (Fuller et al., 1999; Bond et al., 2006). The fact that coating can increase absorption has been confirmed in ambient studies (Wei et al., 2013b; Liu et al., 2015), and the coating may also be responsible for the decrease of parameter  $k$ ; the possible mechanism would be the increase in SSA and decrease of the backscatter fraction caused by the coating (Virkkula et al., 2015). In Payerne, the differences between high and low  $k_6$  are not clearly appreciable, which can be explained by a different meteorology and orography. Indeed, the station is located between the Jura Mountains and the Alps, where the air is in general more stagnant compared to Paris and is channeled from southwest to northeast due to the mountain ranges. This limits the interpretation of our PSCF results and should be further investigated on a longer temporal scale (e.g., several months),

which would provide more representative results for this station.

### 3.6 Influence of the mixing state on the filter-loading effect: removing the coating of ambient aerosols

Our coating hypothesis was put to a definite test during the Ljubljana campaign; we investigated the effect of the ambient aerosol coating thickness reduction on the loading effect. The campaign was carried out in summer, when the atmospheric mixing is stronger, so we expected aged and internally mixed aerosols to be ubiquitous. We have used two approaches to reduce the coating thickness: drying and thermo-denuding the inlet stream. Drying is expected to influence particles coated with hygroscopic material; thermo-denuding was used to remove certain organic compounds (Huffman et al., 2009; Cappa and Wilson, 2012; Liu et al., 2015), but it also removes nitrates and sulfates which decompose above 280 °C (CRC, 1920). The thermo-denuder in our experiment was set to an operation temperature of 300 °C. At this temperature, part of the low-volatility oxygenated organic aerosols (LV-OOAs) is not removed from the sample (Poulain et al., 2014).

The de-coating efficiency of the thermo-denuder was tested using SEM analysis of the impactor samples taken during midday, the time when a well-mixed atmosphere is expected. Coating residues were most pronounced for above-average size particles (Fig. S4); thus the impactor stage with a 170–260 nm particle size range was selected for the analysis (Fig. 10). We can observe soot agglomerates (white patches marked by red arrows), organic residues (dark patches around agglomerates) and brain-shaped dendritic residues (marked by yellow arrows). Dark patches around soot agglomerates can be also found on the thermo-denuded sample, indicating low volatility of these compounds. The main difference between the non-perturbed and thermo-denuded sample is the removal of the dendrite-shaped residue; a similarly shaped residue has been reported in different studies (Buseck and Posfai, 1999; Adachi et al., 2014) as secondary ammonium sulfate particles. To confirm the presence of secondary inorganic particles and analyze their chemical composition, we utilized EDX spectroscopy. In the background area (Fig. 10c, spectrum 1), we identified spectral peaks specific for carbon, oxygen and aluminum, as expected for impactor aluminum foil covered with a thin layer of grease. In the residue area (spectrum 2) we observed carbon and oxygen peaks with higher amplitude than in the background area, and additional sulfur and nitrogen peaks. This indicates the presence of oxidized organic compounds, ammonium sulfate and possibly nitrates, further confirming the presence of coatings and in line with findings of previous studies (Adachi et al., 2014).

The de-coating experiment consisted of four instruments sampling ambient, dried, thermo-denuded, and thermo-denuded and dried air streams simultaneously. The diurnal

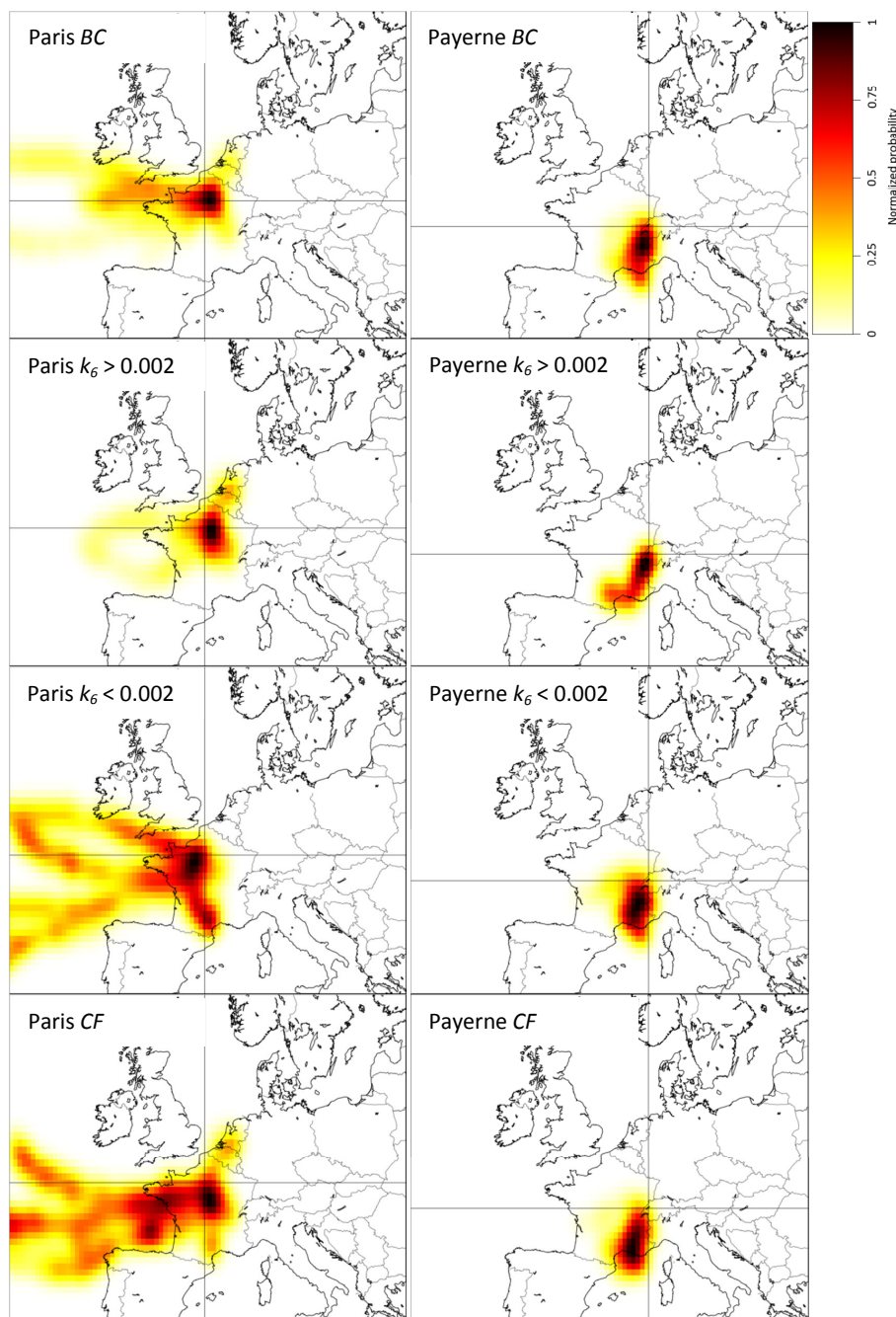


**Figure 9.** Potential source contribution function analysis in Paris and Payerne for measurement with low/high values of the filter-loading compensation parameter  $k_6$ , for the CF and BC being higher than the 75th percentile.

profiles of  $k_6$  show qualitative and quantitative differences between the four treatments (Fig. 11): the loading parameter  $k_6$  for ambient aerosols reaches its highest value during the night and decreases during the afternoon, when the atmosphere is completely mixed. Drying increases the average value of parameter  $k_6$  and amplifies the night–day variation. For the thermo-denuded samples,  $k_6$  is almost constant during the day, with higher average values for the thermo-

denuded and dried sample stream. The average campaign value of parameter  $k_6$  shows a statistically significant difference between all treatments ( $p = 0.05$ ). The  $k_6$  for thermo-denuded samples is similar to that of fresh diesel exhaust (Table 1) as expected for ambient aerosol after removal of inorganic coating by the thermo-denuder. These results are consistent with the findings of the coating factor analysis above, where coating causes reduction of  $k_6$ .

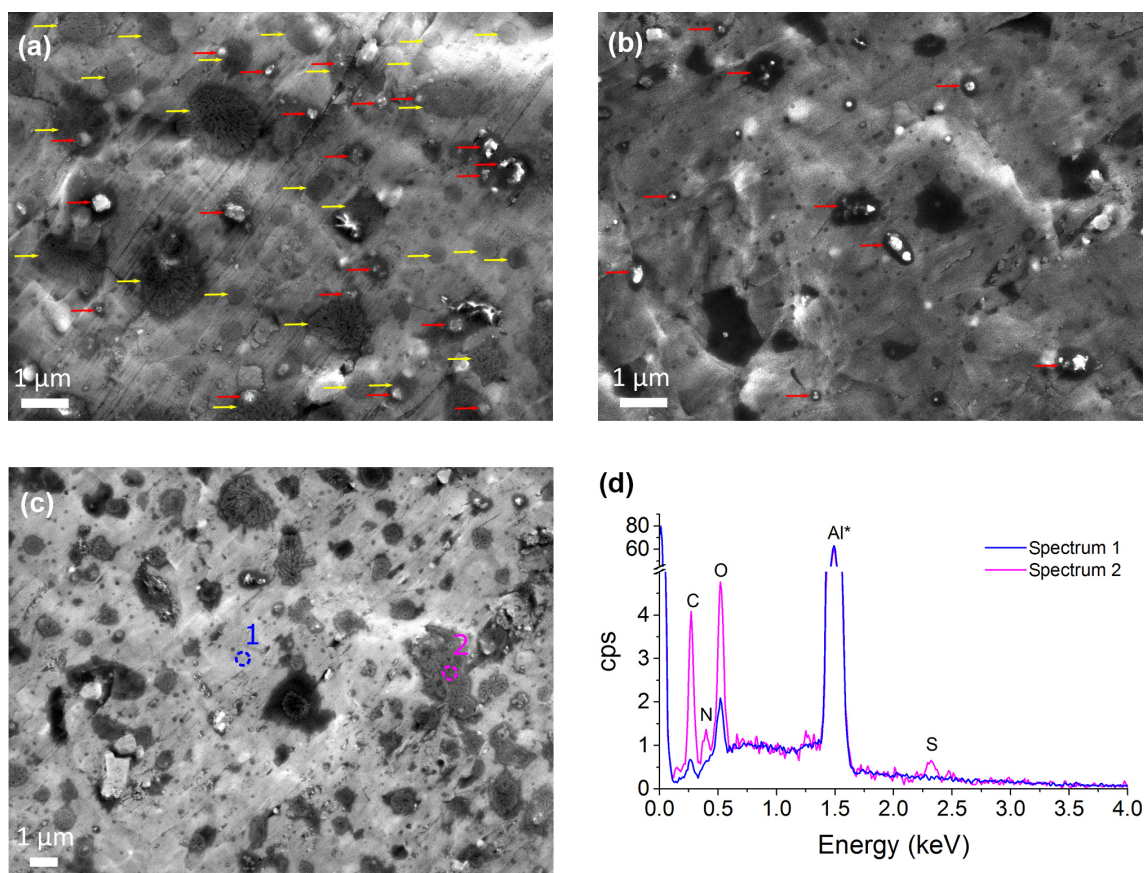


**Figure 10.** SEM images of ambient (a, c) and thermo-denuded (b) impactor samples (size range 170–260 nm) taken during the Ljubljana campaign. The energy-dispersive X-ray spectra (d) were obtained at the selected areas on image (c). Red and yellow arrows mark soot agglomerates and secondary ammonium sulfate residues, respectively.

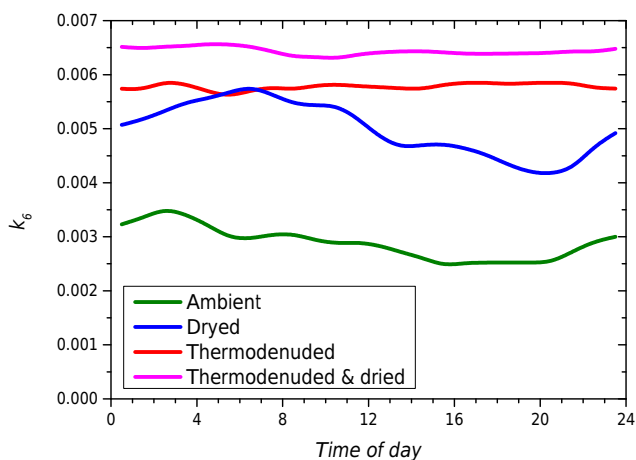


**Figure 11.** Influence of dried and/or thermo-denuded ambient aerosols on the filter-loading parameter  $k_6$  – diurnal plot. The average values of  $k_6$  for the different treatments are significantly different with  $p = 0.05$ .

Freshly emitted BC particles are hydrophobic (Weingartner et al., 1997; Zuberi et al., 2005) and show low relative-humidity-induced particle growth (Laborde et al., 2013). Immediately after sunrise, soot particles in the atmosphere begin to age by developing a coating of secondary species including ammonium nitrate, sulfate and organics (Moffet and Prather, 2009). This coating makes particles hydrophilic and sensitive to relative-humidity-induced growth (Hu et al., 2010; Zhang et al., 2015), which influences scattering and absorption (Wei et al., 2013a, b). Drying the inlet stream during the Ljubljana campaign reduced the thickness of the hydrophilic coating and caused a large increase of  $k_6$ . An even greater effect was observed for the thermo-denuded sample, where most of the inorganic coatings were removed. Interestingly, we observed the effect of drying also for thermo-denuded particles. This is attributed to the presence of oxygenated organic aerosols that are less efficiently removed because of their low volatility (Huffman et al., 2009; Cappa and Jimenez, 2010; Poulain et al., 2014). For the urban environment, it was shown that most of the secondary (oxygenated) organic aerosols are water-soluble (Kondo et al., 2007) and could be prone to relative-humidity-induced growth. This ex-

periment further supports the hypothesis that coating is responsible for the reduction of the filter-loading effect in the Aethalometer.

#### 4 Conclusions

We have tested the hypothesis that the filter-loading effect present in filter-based photometers used for BC determination depends on the optical properties of particles present in the filter matrix, especially on coatings of black carbon particles. High-time-resolution measurements of the filter-loading parameter in the Aethalometer show daily and seasonal variations of the effect, which is most pronounced in the infrared region used for the determination of the black carbon mass concentrations. The filter-loading parameter value increases with the absorption Ångström exponent. It is suggested that this effect is related to the size of the black carbon agglomerates. The loading parameter for fresh combustion products seems to be influenced by the size of the combustion particles, with an approximately 15 % increase in the infrared wavelength region for an aerosol mobility diameter increase of about 4 times. On the other hand, we observed a reduction of the filter-loading effect correlated with the availability of the coating material. A high coating factor coincides with a low value of loading parameter, and vice versa. These results show that during summer the coating material causes reduction of the filter-loading effect. There is less or no correlation in winter, which may be a consequence of biomass burning organics being externally mixed with the black carbon. To further test the coating hypothesis, a de-coating experiment using an aerosol drier and thermo-denuder was performed. De-coating the ambient aerosols increases the filter-loading effect, as the coating is reduced or removed. The coating composed of ammonium sulfate and secondary organics seems to be responsible for the variation of the loading effect. The potential source contribution function analysis shows that high values of the filter-loading parameter in the infrared are indicative of local pollution, whereas low values of the filter-loading parameter result from ageing and coating during long-range transport. Our results show that the filter-loading parameter can be used as a proxy for the determination of the particle coating, thus allowing for differentiation between local/fresh and transported/aged particles. Thus not only is the filter-loading parameter important for compensation of the Aethalometer absorption data, but it also provides additional information on the physical properties of the aerosols.

*Data availability.* The data from ambient measurements are available at, have been submitted to or will be submitted to the public repository EBAS, managed by NILU: <http://ebas.nilu.no/default.aspx> according to the EBAS and respective project (for example ACTRIS) data policy.

**The Supplement related to this article is available online at doi:10.5194/amt-10-1043-2017-supplement.**

*Competing interests.* Luka Drinovec and Griša Močnik are employed by the company Aerosol d.o.o., which develops and manufactures aerosol instrumentation, including the Aethalometer AE33 and the drier used in the campaigns. Hans Moosmüller is a co-inventor of the photoacoustic instruments (PASS and PAX) manufactured by Droplet Measurement Technologies and receives licensing fees from their sale.

*Acknowledgements.* The work described herein was supported by

- EUROSTARS grant E14825 FC Aeth;
- JR-KROP grant 3211-11-000519;
- JR-RK grant 3330-14-509063;
- ACTRIS EU-FP7 grant no. 262254;
- “PREQUALIF” project (ADEME contract no. 1132C0020), DIM R2DS (AAP 2010);
- “PARTICUL’AIR” project, and institutions CNRS, CEA and FEON;
- National Science Foundation (NSF) under Cooperative Support Agreement No. EPS-0814372;
- NASA EPSCoR under Cooperative Agreement No. NNX14AN24A;
- NASA ROSES under grant no. NNX15AI48G;
- NSF under grant no. AGS-1544425.

We thank the Slovenian Environmental Agency and AMES d.o.o. for the use of their measurement sites.

Edited by: W. Maenhaut

Reviewed by: three anonymous referees

#### References

- Adachi, K., Zaizen, Y., Kajino, M., and Igarashi, Y.: Mixing state of regionally transported soot particles and the coating effect on their size and shape at a mountain site in Japan, *J. Geophys. Res.*, 119, 5386–5396, doi:10.1002/2013JD020880, 2014.
- Ångström, A.: On the atmospheric transmission of sun radiation and on dust in the air, *Geogr. Ann.*, 11, 156–166, doi:10.2307/519399, 1929.
- Arnott, W. P., Hamasha, K., Moosmüller, H., Sheridan P. J., and Ogren, J. A.: Towards aerosol light-absorption measurements with a 7-wavelength aethalometer: evaluation with a photoacoustic instrument and 3-wavelength nephelometer, *Aerosol Sci. Tech.*, 39, 17–29, doi:10.1080/027868290901972, 2005.
- Bond, T. C., Anderson, T. L., and Campbell, D.: Calibration and intercomparison of filter-based measurements of visible light absorption by aerosols, *Aerosol Sci. Tech.*, 30, 582–600, doi:10.1080/027868299304435, 1999.
- Bond, T. C., Habib, G., and Bergstrom, R. W.: Limitations in the enhancement of visible light absorption due to mixing state, *J. Geophys. Res.*, 111, D20211, doi:10.1029/2006JD007315, 2006.

- Bond, T. C., Doherty, S. J., Fahey, D. W., Forster, P. M., Bernsten, T., DeAngelo, B. J., Flanner, M. G., Ghan, S., Kärcher, B., Koch, D., Kinne, S., Kondo, Y., Quinn, P. K., Sarofim, M. C., Schultz, M. G., Schulz, M., Venkataraman, C., Zhang, H., Zhang, S., Bellouin, N., Guttikunda, S. K., Hopke, P. K., Jacobson, M. Z., Kaiser, J. W., Klimont, Z., Lohmann, U., Schwarz, J. P., Shindell, D., Storelvmo, T., Warren, S. G., and Zender, C. S.: Bounding the role of black carbon in the climate system: a scientific assessment, *J. Geophys. Res.*, 118, 5380–5552, doi:10.1002/jgrd.50171, 2013.
- Bressi, M., Sciare, J., Ghersi, V., Bonnaire, N., Nicolas, J. B., Petit, J.-E., Moukhtar, S., Rosso, A., Mihalopoulos, N., and Féron, A.: A one-year comprehensive chemical characterisation of fine aerosol (PM<sub>2.5</sub>) at urban, suburban and rural background sites in the region of Paris (France), *Atmos. Chem. Phys.*, 13, 7825–7844, doi:10.5194/acp-13-7825-2013, 2013.
- Bressi, M., Sciare, J., Ghersi, V., Mihalopoulos, N., Petit, J.-E., Nicolas, J. B., Moukhtar, S., Rosso, A., Féron, A., Bonnaire, N., Poulakis, E., and Theodosi, C.: Sources and geographical origins of fine aerosols in Paris (France), *Atmos. Chem. Phys.*, 14, 8813–8839, doi:10.5194/acp-14-8813-2014, 2014.
- Bruns, E. A., Krapf, M., Orasche, J., Huang, Y., Zimmermann, R., Drinovec, L., Močnik, G., El-Haddad, I., Slowik, J. G., Dommen, J., Baltensperger, U., and Prévôt, A. S. H.: Characterization of primary and secondary wood combustion products generated under different burner loads, *Atmos. Chem. Phys.*, 15, 2825–2841, doi:10.5194/acp-15-2825-2015, 2015.
- Buseck, P. R. and Posfai, M.: Airborne minerals and related aerosol particles: Effects on climate and the environment, *P. Natl. Acad. Sci. USA*, 96, 3372–3379, doi:10.1073/pnas.96.7.3372, 1999.
- Canagaratna, M. R., Jayne, J. T., Jimenez, J. L., Allan, J. D., Alfarra, M. R., Zhang, Q., Onasch, T. B., Drewnick, F., Coe, H., Middlebrook, A., Delia, A., Williams, L. R., Trimborn, A. M., Northway, M. J., DeCarlo, P. F., Kolb, C. E., Davidovits, P., and Worsnop, D. R.: Chemical and microphysical characterization of ambient aerosols with the aerodyne aerosol mass spectrometer, *Mass Spectrom. Rev.*, 26, 185–222, doi:10.1002/mas.20115, 2007.
- Cappa, C. D. and Jimenez, J. L.: Quantitative estimates of the volatility of ambient organic aerosol, *Atmos. Chem. Phys.*, 10, 5409–5424, doi:10.5194/acp-10-5409-2010, 2010.
- Cappa, C. D. and Wilson, K. R.: Multi-generation gas-phase oxidation, equilibrium partitioning, and the formation and evolution of secondary organic aerosol, *Atmos. Chem. Phys.*, 12, 9505–9528, doi:10.5194/acp-12-9505-2012, 2012.
- Chakrabarty, R. K., Arnold, I. J., Francisco, D. M., Hatchett, B., Hosseinpour, F., Loria, M., Pokharel, A., and Woody, B. M.: Black and brown carbon fractal aggregates from combustion of two fuels widely used in Asian rituals, *J. Quant. Spectrosc. Ra.*, 122, 25–30, doi:10.1016/j.jqsrt.2012.12.011, 2013.
- Chakrabarty, R. K., Beres, N. D., Moosmüller, H., China, S., Mazzoleni, C., Dubey, M. K., Liu, L., and Mishchenko, M. I.: Soot superaggregates from flaming wildfires and their direct radiative forcing, *Nat. Sci. Rep.*, 4, 5508, doi:10.1038/srep05508, 2014.
- Chen, L.-W. A., Moosmüller, H., Arnott, W. P., Chow, J. C., Watson, J. G., Susott, R. A., Babbitt, R. E., Wold, C. E., Lincoln, E. N., and Hao, W. M.: Emissions from laboratory combustion of wildland fuels: emission factors and source profiles, *Environ. Sci. Technol.*, 41, 4317–4325, doi:10.1021/es062364i, 2007.
- China, S., Mazzoleni, C., Gorkowski, K., Allison, C. A., and Dubey, M. K.: Morphology and mixing state of individual freshly emitted wildfire carbonaceous particles, *Nat. Commun.*, 4, 2122, doi:10.1038/ncomms3122, 2013.
- Collaud Coen, M., Weingartner, E., Apituley, A., Ceburnis, D., Fierz-Schmidhauser, R., Flentje, H., Henzing, J. S., Jennings, S. G., Moerman, M., Petzold, A., Schmid, O., and Baltensperger, U.: Minimizing light absorption measurement artifacts of the Aethalometer: evaluation of five correction algorithms, *Atmos. Meas. Tech.*, 3, 457–474, doi:10.5194/amt-3-457-2010, 2010.
- CRC: Handbook of Chemistry and Physics, 8th edition, CRC Press, Cleveland, Ohio, USA, 1920.
- Crenn, V., Sciare, J., Croteau, P. L., Verlhac, S., Fröhlich, R., Belis, C. A., Aas, W., Äijälä, M., Alastuey, A., Artiñano, B., Baisnée, D., Bonnaire, N., Bressi, M., Canagaratna, M., Canonaco, F., Carbone, C., Cavalli, F., Coz, E., Cubison, M. J., Esser-Gietl, J. K., Green, D. C., Gros, V., Heikkinen, L., Herrmann, H., Lunder, C., Minguillón, M. C., Močnik, G., O'Dowd, C. D., Ovadnevaite, J., Petit, J.-E., Petralia, E., Poulain, L., Priestman, M., Riffault, V., Ripoll, A., Sarda-Estève, R., Slowik, J. G., Setyan, A., Wiedensohler, A., Baltensperger, U., Prévôt, A. S. H., Jayne, J. T., and Favez, O.: ACTRIS ACSM intercomparison – Part 1: Reproducibility of concentration and fragment results from 13 individual Quadrupole Aerosol Chemical Speciation Monitors (Q-ACSM) and consistency with co-located instruments, *Atmos. Meas. Tech.*, 8, 5063–5087, doi:10.5194/amt-8-5063-2015, 2015.
- Crippa, M., El Haddad, I., Slowik, J. G., DeCarlo, P. F., Mohr, C., Heringa, M. F., Chirico, R., Marchand, N., Sciare, J., Baltensperger, U., and Prevot, A. S. H.: Identification of marine and continental aerosol sources in Paris using high resolution aerosol mass spectrometry, *J. Geophys. Res.*, 118, 1950–1963, doi:10.1002/jgrd.50151, 2013.
- Drinovec, L., Močnik, G., Zotter, P., Prévôt, A. S. H., Ruckstuhl, C., Coz, E., Rupakheti, M., Sciare, J., Müller, T., Wiedensohler, A., and Hansen, A. D. A.: The “dual-spot” Aethalometer: an improved measurement of aerosol black carbon with real-time loading compensation, *Atmos. Meas. Tech.*, 8, 1965–1979, doi:10.5194/amt-8-1965-2015, 2015.
- Favez, O., Cachier, H., Sciare, J., Sarda-Estève, R., and Martinon, L.: Evidence for a significant contribution of wood burning aerosols to PM<sub>2.5</sub> during the winter season in Paris, France, *Atmos. Environ.*, 43, 3640–3644, doi:10.1016/j.atmosenv.2009.04.035, 2009.
- Freutel, F., Schneider, J., Drewnick, F., von der Weiden-Reinmüller, S.-L., Crippa, M., Prévôt, A. S. H., Baltensperger, U., Poulain, L., Wiedensohler, A., Sciare, J., Sarda-Estève, R., Burkhardt, J. F., Eckhardt, S., Stohl, A., Gros, V., Colomb, A., Michoud, V., Doussin, J. F., Borbon, A., Haefelin, M., Morille, Y., Beekmann, M., and Borrmann, S.: Aerosol particle measurements at three stationary sites in the megacity of Paris during summer 2009: meteorology and air mass origin dominate aerosol particle composition and size distribution, *Atmos. Chem. Phys.*, 13, 933–959, doi:10.5194/acp-13-933-2013, 2013.
- Fröhlich, R., Cubison, M. J., Slowik, J. G., Bukowiecki, N., Prévôt, A. S. H., Baltensperger, U., Schneider, J., Kimmel, J. R., Gonin, M., Rohner, U., Worsnop, D. R., and Jayne, J. T.: The ToF-ACSM: a portable aerosol chemical speciation monitor

- with TOFMS detection, *Atmos. Meas. Tech.*, 6, 3225–3241, doi:10.5194/amt-6-3225-2013, 2013.
- Fröhlich, R., Crenn, V., Setyan, A., Belis, C. A., Canonaco, F., Favez, O., Riffault, V., Slowik, J. G., Aas, W., Aijälä, M., Alastuey, A., Artiñano, B., Bonnaire, N., Bozzetti, C., Bressi, M., Carbone, C., Coz, E., Croteau, P. L., Cubison, M. J., Esser-Gietl, J. K., Green, D. C., Gros, V., Heikkinen, L., Herrmann, H., Jayne, J. T., Lunder, C. R., Minguillón, M. C., Močnik, G., O'Dowd, C. D., Ovadnevaite, J., Petralia, E., Poulain, L., Priestman, M., Ripoll, A., Sarda-Estève, R., Wiedensohler, A., Baltensperger, U., Sciare, J., and Prévôt, A. S. H.: ACTRIS ACSM intercomparison – Part 2: Intercomparison of ME-2 organic source apportionment results from 15 individual, co-located aerosol mass spectrometers, *Atmos. Meas. Tech.*, 8, 2555–2576, doi:10.5194/amt-8-2555-2015, 2015.
- Fuller, K. A., Malm, W. C., and Kreidenweis, S. M.: Effects of mixing on extinction by carbonaceous particles, *J. Geophys. Res.*, 104, 941–915, doi:10.1029/1998JD100069, 1999.
- Grahame, T. J., Klemm, R., and Schlesinger, R. B.: Public health and components of particulate matter: The changing assessment of black carbon, *J. Air Waste Manage.*, 64, 620–660, doi:10.1080/10962247.2014.912692, 2014.
- Harris, S. J. and Maricq, M. M.: Signature size distributions for diesel and gasoline engine exhaust particulate matter, *J. Aerosol Sci.*, 32, 749–764, doi:10.1016/S0021-8502(00)00111-7, 2001.
- Healy, R. M., Sciare, J., Poulain, L., Crippa, M., Wiedensohler, A., Prévôt, A. S. H., Baltensperger, U., Sarda-Estève, R., McGuire, M. L., Jeong, C.-H., McGillicuddy, E., O'Connor, I. P., Sodeau, J. R., Evans, G. J., and Wenger, J. C.: Quantitative determination of carbonaceous particle mixing state in Paris using single-particle mass spectrometer and aerosol mass spectrometer measurements, *Atmos. Chem. Phys.*, 13, 9479–9496, doi:10.5194/acp-13-9479-2013, 2013.
- Hu, D., Qiao, L., Chen, J., Ye, X., Yang, X., Cheng, T., and Fang, W.: Hygroscopicity of inorganic aerosols: Size and relative humidity effects on the growth factor, *Aerosol Air Qual. Res.*, 10, 255–264, doi:10.4209/aaqr.2009.12.0076, 2010.
- Huffman, J. A., Docherty, K. S., Aiken, A. C., Cubison, M. J., Ulbrich, I. M., DeCarlo, P. F., Sueper, D., Jayne, J. T., Worsnop, D. R., Ziemann, P. J., and Jimenez, J. L.: Chemically-resolved aerosol volatility measurements from two megacity field studies, *Atmos. Chem. Phys.*, 9, 7161–7182, doi:10.5194/acp-9-7161-2009, 2009.
- Hyyvärinen, A.-P., Vakkari, V., Laakso, L., Hooda, R. K., Sharma, V. P., Panwar, T. S., Beukes, J. P., van Zyl, P. G., Josipovic, M., Garland, R. M., Andreae, M. O., Pöschl, U., and Petzold, A.: Correction for a measurement artifact of the Multi-Angle Absorption Photometer (MAAP) at high black carbon mass concentration levels, *Atmos. Meas. Tech.*, 6, 81–90, doi:10.5194/amt-6-81-2013, 2013.
- Jacobson, M. Z.: A physically-based treatment of elemental carbon optics: Implications for global direct forcing of aerosols, *Geophys. Res. Lett.*, 27, 217–220, doi:10.1029/1999GL010968, 2000.
- Jacobson, M. Z.: Strong radiative heating due to the mixing state of black carbon in atmospheric aerosols, *Nature*, 409, 695–697, doi:10.1038/35055518, 2001.
- Janssen, N. A. H., Hoek, G., Simic-Lawson, M., Fischer, P., van Bree, L., Ten Brink, H., Keuken, M., Atkinson, R. W., Anderson, H. R., Brunekreef, B., and Cassee, F. R.: Black carbon as an additional indicator of the adverse health effects of airborne particles compared with PM<sub>10</sub> and PM<sub>2.5</sub>, *Environ. Health Persp.*, 119, 1691–1699, doi:10.1289/ehp.1003369, 2011.
- Janssen, N. A. H., Gerlofs-Nijland, M. E., Lanki, T., Salonen, R. O., Cassee, F., Hoek, G., Fischer, P., Brunekreef, B., and Krzyzanowski, M.: Health effects of black carbon, The WHO European Centre for Environment and Health, Bonn, Germany, World Health Organisation Regional Office for Europe, Copenhagen, Denmark, 2012.
- Keskinen, J. and Rönkkö, T.: Can real-world diesel exhaust particle size distribution be reproduced in the laboratory? A critical review, *J. Air Waste Manage.*, 60, 1245–1255, doi:10.3155/1047-3289.60.10.1245, 2010.
- Kirchstetter, T. W., Novakov, T., and Hobbs, P. V.: Evidence that the spectral dependence of light absorption by aerosols is affected by organic carbon, *J. Geophys. Res.*, 109, D21208, doi:10.1029/2004JD004999, 2004.
- Kondo, Y., Miyazaki, Y., Takegawa, N., Miyakawa, T., Weber, R. J., Jimenez, J. L., Zhang, Q., and Worsnop, D. R.: Oxygenated and water-soluble organic aerosols in Tokyo, *J. Geophys. Res.*, 112, D01203, doi:10.1029/2006JD007056, 2007.
- Laborde, M., Crippa, M., Tritscher, T., Jurányi, Z., Decarlo, P. F., Temime-Roussel, B., Marchand, N., Eckhardt, S., Stohl, A., Baltensperger, U., Prévôt, A. S. H., Weingartner, E., and Gysel, M.: Black carbon physical properties and mixing state in the European megacity Paris, *Atmos. Chem. Phys.*, 13, 5831–5856, doi:10.5194/acp-13-5831-2013, 2013.
- Lack, D. A., Moosmüller, H., McMeeking, G. R., Chakrabarty, R. K., and Baumgardner, D.: Characterizing elemental, equivalent black, and refractory black carbon aerosol particles: a review of techniques, their limitations and uncertainties, *Anal. Bioanal. Chem.*, 406, 99–122, doi:10.1007/s00216-013-7402-3, 2014.
- Lewis, K., Arnott, W. P., Moosmüller, H., and Wold, C. E.: Strong spectral variation of biomass smoke light absorption and single scattering albedo observed with a novel dual-wavelength photoacoustic instrument, *J. Geophys. Res.*, 113, D16203, doi:10.1029/2007JD009699, 2008.
- Liu, S., Aiken, A. C., Gorkowski, K., Dubey, M. K., Cappa, C. D., Williams, L. R., Herndon, S. C., Massoli, P., Fortner, E. C., Chhabra, P. S., Brooks, W. A., Onasch, T. B., Jayne, J. T., Worsnop, D. R., China, S., Sharma, N., Mazzoleni, C., Xu, L., Ng, N. L., Liu, D., Allan, J. L., Lee, J. D., Fleming, Z. L., Mohr, C., Zotter, P., Szidat, S., and Prévôt, A. S. H.: Enhanced light absorption by mixed source black and brown carbon particles in UK winter, *Nat. Commun.* 6, 8435, doi:10.1038/ncomms9435, 2015.
- Moffet, R. C. and Prather, K. A.: In-situ measurements of the mixing state and optical properties of soot with implications for radiative forcing estimates, *P. Natl. Acad. Sci. USA*, 106, 11872–11877, doi:10.1073/pnas.0900040106, 2009.
- Moosmüller, H., Chakrabarty, R. K., and Arnott, W. P.: Aerosol light absorption and its measurement: a review, *J. Quant. Spectrosc. Ra.*, 110, 844–878, doi:10.1016/j.jqsrt.2009.02.035, 2009.
- Ng, N. L., Herndon, S. C., Trimborn, A., Canagaratna, M. R., Croteau, P. L., Onasch, T. B., Sueper, D., Worsnop, D. R., Zhang, Q., and Sun, Y. L.: An aerosol chemical speciation monitor (ACSM) for routine monitoring of the composition and mass

- concentrations of ambient aerosol, *Aerosol Sci. Tech.*, 45, 780–794, 2011.
- Ning, Z., Chan, K. L., Wong, K. C., Westerdahl, D., Močnik, G., Zhou, J. H., and Cheung, C. S.: Black carbon mass size distributions of diesel exhaust and urban aerosols measured using differential mobility analyzer in tandem with Aethalometer, *Atmos. Environ.*, 80, 31–40, doi:10.1080/02786820500543324, 2013.
- Olstrup, H., Johansson, C., and Forsberg, B.: The use of carbonaceous particle exposure metrics in health impact calculations, *Int. J. Environ. Res. Public Health*, 13, 249, doi:10.3390/ijerph13030249, 2016.
- Pagels, J., Dutcher, D. D., Stolzenburg, M. R., McMurry, P. H., Gälli, M. E., and Gross, D. S.: Fine-particle emissions from solid biofuel combustion studied with single-particle mass spectrometry: Identification of markers for organics, soot, and ash components, *J. Geophys. Res.*, 118, 859–870, doi:10.1029/2012JD018389, 2013.
- Park, S. S., Hansen, A. D. A., and Cho, Y.: Measurement of real time black carbon for investigating spot loading effects of Aethalometer data, *Atmos. Environ.*, 11, 1449–1455, doi:10.1016/j.atmosenv.2010.01.025, 2010.
- Petit, J.-E., Favez, O., Sciare, J., Canonaco, F., Croteau, P., Močnik, G., Jayne, J., Worsnop, D., and Leoz-Garziandia, E.: Submicron aerosol source apportionment of wintertime pollution in Paris, France by double positive matrix factorization (PMF<sup>2</sup>) using an aerosol chemical speciation monitor (ACSM) and a multi-wavelength Aethalometer, *Atmos. Chem. Phys.*, 14, 13773–13787, doi:10.5194/acp-14-13773-2014, 2014.
- Petit, J.-E., Favez, O., Sciare, J., Crenn, V., Sarda-Estève, R., Bonnaire, N., Močnik, G., Dupont, J.-C., Haeffelin, M., and Leoz-Garziandia, E.: Two years of near real-time chemical composition of submicron aerosols in the region of Paris using an Aerosol Chemical Speciation Monitor (ACSM) and a multi-wavelength Aethalometer, *Atmos. Chem. Phys.*, 15, 2985–3005, doi:10.5194/acp-15-2985-2015, 2015.
- Polissar, A. V., Hopke, P. K., Paatero, P., Kaufmann, Y. J., Hall, D. K., Bodhaine, B. A., Dutton, E. G., and Harris, J. M.: The aerosol at Barrow, Alaska: long-term trends and source locations, *Atmos. Environ.*, 33, 2441–2458, doi:10.1016/S1352-2310(98)00423-3, 1999.
- Poulain, L., Birmili, W., Canonaco, F., Crippa, M., Wu, Z. J., Nordmann, S., Spindler, G., Prévôt, A. S. H., Wiedensohler, A., and Herrmann, H.: Chemical mass balance of 300 °C non-volatile particles at the tropospheric research site Melpitz, Germany, *Atmos. Chem. Phys.*, 14, 10145–10162, doi:10.5194/acp-14-10145-2014, 2014.
- Sandradewi, J., Prévôt, A. S. H., Szidat, S., Perron, N., Alfarra, M. R., Lanz, V. A., Weingartner, E., and Baltensperger, U.: Using aerosol light absorption measurements for the quantitative determination of wood burning and traffic emission contributions to particulate matter, *Environ. Sci. Technol.*, 42, 3316–3323, doi:10.1021/es702253m, 2008.
- Schmid, O., Artaxo, P., Arnott, W. P., Chand, D., Gatti, L. V., Frank, G. P., Hoffer, A., Schnaiter, M., and Andreae, M. O.: Spectral light absorption by ambient aerosols influenced by biomass burning in the Amazon Basin. I: Comparison and field calibration of absorption measurement techniques, *Atmos. Chem. Phys.*, 6, 3443–3462, doi:10.5194/acp-6-3443-2006, 2006.
- Schnaiter, M., Horvath, H., Mohler, O., Naumann, K. H., Saathoff, H., and Schock, O. W.: UV-VIS-NIR spectral optical properties of soot and soot-containing aerosols, *J. Aerosol Sci.*, 34, 1421–1444, doi:10.1016/S0021-8502(03)00361-6, 2003.
- Segura, S., Estellés, V., Titos, G., Lyamani, H., Utrillas, M. P., Zotter, P., Prévôt, A. S. H., Močnik, G., Alados-Arboledas, L., and Martínez-Lozano, J. A.: Determination and analysis of in situ spectral aerosol optical properties by a multi-instrumental approach, *Atmos. Meas. Tech.*, 7, 2373–2387, doi:10.5194/amt-7-2373-2014, 2014.
- Seinfeld, J. H. and Pandis, S. N.: *Atmospheric Chemistry and Physics: From Air Pollution to Climate Change*, John Wiley and Sons 2006, Hoboken, New Jersey, USA, 2006.
- Shindell, D., Kuylenstierna, J. C. I., Vignati, E., van Dingenen, R., Amann, M., Klimont, Z., Anenberg, S. C., Müller, N., Janssens-Maenhout, G., Raes, F., Schwartz, J., Faluvegi, G., Pozzoli, L., Kupiainen, K., Höglund-Isaksson, L., Emberson, L., Streets, D., Ramanathan, V., Hicks, K., Oanh, N. T. K., Milly, G., Williams, M., Demkine, V., and Fowler, D.: Simultaneously mitigating near-term climate change and improving human health and food security, *Science*, 335, 183–189, doi:10.1126/science.1210026, 2012.
- Shiraiwa, M., Kondo, Y., Moteki, N., Takegawa, N., Sahu, L. K., Takami, A., Hatakeyama, S., Yonemura, S., and Blake, D. R.: Radiative impact of mixing state of black carbon aerosol in Asian outflow, *J. Geophys. Res.*, 113, D24210, doi:10.1029/2008JD010546, 2008.
- Smith, K. R., Jerrett, M., Anderson, H. R., Burnett, R. T., Stone, V., Derwent, R., Atkinson, R. W., Cohen, A., Shonkoff, S. B., Krewski, D., Pope, C. A., Thun, M. J., and Thurston, G.: Public health benefits of strategies to reduce greenhouse-gas emissions: health implications of short-lived greenhouse pollutants, *Lancet*, 374, 2091–2103, doi:10.1016/S0140-6736(09)61716-5, 2009.
- Stein, A. F., Draxler, R. R., Rolph, G. D., Stunder, B. J. B., Cohen, M. D., and Ngan, F.: NOAA's HYSPLIT atmospheric transport and dispersion modeling system, *B. Am. Meteorol. Soc.*, 96, 2059–2077, doi:10.1175/BAMS-D-14-00110.1, 2015.
- Tian, J., Chow, J. C., Cao, J., Han, Y., Ni, H., Chen, L. W. A., Wang, X., Huang, R., Moosmüller, H., and Watson, J. G.: A biomass combustion chamber: design, evaluation, and a case study of wheat straw combustion emission tests, *Aerosol Air Qual. Res.*, 15, 2104–2114, doi:10.4209/aaqr.2015.03.0167, 2015.
- Virkkula, A., Mäkelä, T., Hillamo, R., Yli-Tuomi, T., Hirsikko, A., Hämeri, K., and Koponen, I. K.: A simple procedure for correcting loading effects of Aethalometer data, *J. Air Waste Manage.*, 57, 1214–1222, doi:10.3155/1047-3289.57.10.1214, 2007.
- Virkkula, A., Chi, X., Ding, A., Shen, Y., Nie, W., Qi, X., Zheng, L., Huang, X., Xie, Y., Wang, J., Petäjä, T., and Kulmala, M.: On the interpretation of the loading correction of the aethalometer, *Atmos. Meas. Tech.*, 8, 4415–4427, doi:10.5194/amt-8-4415-2015, 2015.
- Waked, A., Favez, O., Alleman, L. Y., Piot, C., Petit, J.-E., Delaunay, T., Verlinden, E., Golly, B., Besombes, J.-L., Jaffrezo, J.-L., and Leoz-Garziandia, E.: Source apportionment of PM<sub>10</sub> in a north-western Europe regional urban background site (Lens, France) using positive matrix factorization and including primary biogenic emissions, *Atmos. Chem. Phys.*, 14, 3325–3346, doi:10.5194/acp-14-3325-2014, 2014.

- Wei, Y., Ma, L., Cao, T., Zhang, Q., Wu, J., Buseck, P. R., and Thompson, J. E.: Light scattering and extinction measurements combined with laser-induced incandescence for the real-time determination of soot mass absorption cross section, *Anal. Chem.*, 85, 9181–9188, doi:10.1021/ac401901b, 2013a.
- Wei, Y., Zhang, Q., and Thompson, J. E.: Atmospheric black carbon can exhibit enhanced light absorption at high relative humidity, *Atmos. Chem. Phys. Discuss.*, 13, 29413–29445, doi:10.5194/acpd-13-29413-2013, 2013b.
- Weingartner, E., Burtscher, H., and Baltensperger, U.: Hygroscopic properties of carbon and diesel soot particles, *Atmos. Environ.*, 31, 2311–2327, doi:10.1016/S1352-2310(97)00023-X, 1997.
- Weingartner, E., Saathoff, H., Schnaiter, M., Streit, N., Bitnar, B., and Baltensperger, U.: Absorption of light by soot particles: determination of the absorption coefficient by means of Aethalometers, *J. Aerosol Sci.*, 34, 1445–1463, doi:10.1016/S0021-8502(03)00359-8, 2003.
- Zhang, L., Sun, J. Y., Shen, X. J., Zhang, Y. M., Che, H., Ma, Q. L., Zhang, Y. W., Zhang, X. Y., and Ogren, J. A.: Observations of relative humidity effects on aerosol light scattering in the Yangtze River Delta of China, *Atmos. Chem. Phys.*, 15, 8439–8454, doi:10.5194/acp-15-8439-2015, 2015.
- Zuberi, B., Johnson, K. S., Aleks, G. K., Molina, L. T., Molina, M. J., and Laskin, A.: Hydrophilic properties of aged soot, *Geophys. Res. Lett.*, 32, L01807, doi:10.1029/2004GL021496, 2005.